

Feasibility of Geomagnetic Localization and Geomagnetic RatSLAM

Rafael Berkvens*, Dries Vandermeulen*, Charles Vercauteren*, Herbert Peremans[†], and Maarten Weyn*

*CoSys-Lab, FTI, University of Antwerp, Paardenmarkt 92, B-2000 Antwerp, Belgium

[†]ENM, FTEW, University of Antwerp, Prinsstraat 13, B-2000 Antwerp, Belgium

rafael.berkvens@uantwerpen.be, dries.vandermeulen@student.artesis.be,

{charles.vercauteren, herbert.peremans, maarten.weyn}@uantwerpen.be

Abstract—The need for accurate indoor localization increases as we get used to accessible outdoor localization, and the number of applications depending on localization grows. Indoor localization is challenging because of frequent line of sight obstructions and dynamic changes in the environment. Magnetometers can be found in many modern electronic devices and provide a simple way to measure the geomagnetic field intensity. Due to distortions in this magnetic field, these measurements often provide enough information to enable identification of a location using pattern matching. We show the feasibility of using these magnetic field intensity measurements in localization and SLAM applications. Our SLAM system of choice is the biologically inspired RatSLAM, as it allows pattern matching as scene recognition. We demonstrate a number of experiments in various environments, including a suburban house and a university lab. We conclude that geomagnetic localization and SLAM are feasible in environments with many distortions in the magnetic field. Such locations are easier to identify than locations with little distortions, which will have the same pattern of magnetic field over larger areas.

Keywords—Indoor localization; Indoor SLAM; Magnetic field intensity; Geomagnetic indoor localization; RatSLAM.

I. INTRODUCTION

As we state in our AMBIENT 2013 paper [1], the outdoor global positioning system fails when used indoors. In addition, localization systems based on a single technology are prone to failure [2]. The last decade localization related research is focusing more and more on indoor localization, since most use cases concerning people or asset tracking also require an indoor location estimation.

Indoor localization can be performed by detecting the presence of radio frequency devices, of which Wi-Fi is probably the most common. Such technologies have been developed in an opportunistic sensor fusion system in [3]. These systems can be enhanced by additional localization measurements. The earth's magnetic field is even more ambient than Wi-Fi access points, and research shows that animals use this magnetic field for orientation [4, 5]. This leads to the idea that the earth's magnetic field can be used for indoor localization, a technique referred to as geomagnetic indoor localization.

In the field of geomagnetic indoor localization it is actually the distortions of the magnetic field that are used to find a location [6–11]. These distortions are usually created by concrete buildings, metal objects, electrical wires, etc. Our

own research confirms these findings for different sensors and environments [1].

If a technology can be used for localization, it can often be used for simultaneous localization and mapping (SLAM). In localization, a map of the environment is available, with corresponding localization hints, such as access point locations or signal attenuation patterns [3]. In SLAM, this map is not available but is built simultaneously with the calculation of a path [12, 13]. Typical algorithms of SLAM are Extended Kalman Filter SLAM (EKF-SLAM), such as in [14]; Graph-SLAM, such as in [15], which uses an information matrix; and FastSLAM [16], which uses a Monte Carlo particle filter.

A biologically inspired SLAM variant is RatSLAM [17], which is based on a rat's hippocampus. The hippocampus is the part of the brain where, among other things, the localization and mapping is done. This functionality is mimicked by the RatSLAM algorithm to create semimetric, topological maps of the environment. RatSLAM's original input is a simple web camera, which performed great even when mapping an entire suburb [18]. The camera input has also been replaced by a biomimetic sonar, an algorithm termed BatSLAM [19, 20]. Work has also been done to enable RatSLAM to use other sensors, like laser range finders, depth cameras, and simple sonars, in a sensor fusion system [21]. To summarize, the key difference between geomagnetic localization and geomagnetic RatSLAM is the need for an a priori known magnetic field intensity map for geomagnetic localization, which is not required for geomagnetic RatSLAM as such a map will be built implicitly by the system while exploring the environment.

This paper represents an extension of the work reported on in the paper [1] by applying the sensor model used for localization to the RatSLAM algorithm. This way, we can create maps suitable for geomagnetic indoor localization for a specific environment while simultaneously localizing on that map. Another advantage of such a system is that the magnetic maps used for indoor localization can at all times be kept up to date. Other geomagnetic SLAM approaches exist, one using a Monte Carlo particle filter [22] and another using a SLAM algorithm called FootSLAM [23, 24].

The structure of this paper is as follows. In Section II, we give some background on the earth's magnetic field and details on the RatSLAM algorithm, with a focus on the location recognition process. In Section III, we explain our pattern

matching measurement model. In Section IV, we provide detailed results for both localization and RatSLAM using the earth's magnetic field. In Section V, we come to our conclusion and discuss some of our future work.

II. BACKGROUND

In this section, we discuss the main techniques that support our results, the sensing of the earth's magnetic field. Additionally, we describe how pattern matching localization was performed. Lastly, we explain the RatSLAM algorithm with a focus on the location recognition process.

A. Magnetic field sensing

In this section, we will discuss some issues to consider when measuring the magnetic field. Firstly, we will briefly discuss the magnetic field. Subsequently, we will explain how magnetometers measure this magnetic field and how they are influenced. Lastly, we will focus on the indoor magnetic field intensity, as this is our area of interest.

1) *Magnetic B field*: The earth's magnetic field is commonly called the magnetic B field. It originates from currents in the fluid outer core of the earth, which are created by both temperature, pressure, and composition of the fluid and the spin of the earth [10]. The magnetic B field is defined by its direction and intensity. The direction always points to the magnetic north; the intensity is measured in Tesla [T], and ranges between 22 μ T and 67 μ T according to [25].

The geomagnetic field vector, B_m , has seven components, illustrated in Figure 1. The X intensity's axis points to the geographical north, which is at the north end of the axis around which the earth spins. The Y intensity's axis points to the corresponding geographical east. The Z intensity's axis points to the earth's nadir. Derived from X , Y , and Z are the total intensity F ; the horizontal intensity H , which is the projection of F on the plane described by X and Y ; the inclination I , which is the angle between F and the plane described by X and Y ; and the declination D , which is the angle between X and H [25]. Note that H will point to the magnetic north of the earth, while X points to the geographical north of the earth.

At our location, Antwerp, Belgium, the declination H is $0^\circ 19'$ and inclination I is $66^\circ 25'$. The average total intensity F is 48.73 μ T [1].

2) *Magnetometers*: The geomagnetic field vector B_m can be measured by magnetometers in the form of X' , Y' , and Z' intensities. These intensities are measured along the reference axes of the magnetometer and can only be translated to X , Y , and Z intensities by tilt compensation and turning the X' intensity's axis to the geographical north. Correspondingly, the F and H' intensities can be calculated as the euclidean norm:

$$F = \sqrt{X'^2 + Y'^2 + Z'^2} \quad (1)$$

$$H' = \sqrt{X'^2 + Y'^2} \quad (2)$$

where X' , Y' , Z' , and H' indicate intensities measured relative to the orientation frame of the magnetometer. The

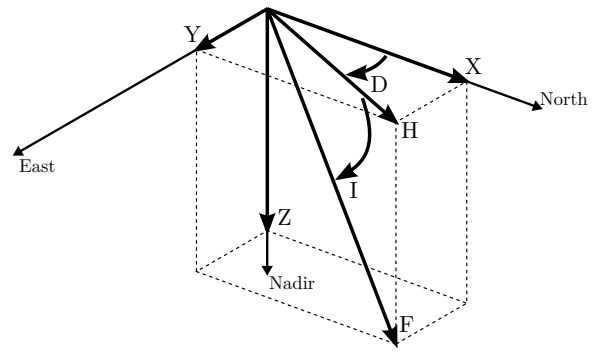


Figure 1. The components of the geomagnetic field vector B_m , based on [25].

F intensity is the same for any orientation. Many recent, high level electronic devices, such as smartphones and tablets, feature magnetometers. This widespread availability of magnetometers makes them attractive to use for localization applications.

For the localization research, we use two different magnetometers on two different platforms. These are a Honeywell HMC5843 magnetometer, found in a Shimmer 9 DOF Kinematic sensor, and a AK9873 magnetometer, found in a Huawei Sonic U8650 smartphone. The behavior of both sensors was tested to determine if the localization performance was platform independent. For the RatSLAM research, a similar sensor is used. This is a AK9863 magnetometer, found in a LG Google Nexus 5 smartphone.

We will repeat here our extensive testing of the sensors used for the localization research [1]. The first test is conducted in an indoor bedroom apartment where both sensors are individually placed on a wooden desk, away from any possible interference factors like metal objects or electronic devices. The sensor sends data back via Bluetooth to a computer where all data was recorded. Both sensors are placed on the desk with their X' intensity's axis manually pointed towards geographical north.

Table I shows the average magnetic field intensity of the first test. Test results show that magnetic field intensity measurements are not the same for both sensor platforms. This can be expected, as both sensors have a unique electronic and metal composition, which might distort sensor readings. These distortions are called hard iron effects and are caused by the internal structure of the sensor. Compensation for these hard iron effects is needed. If no compensation for hard iron effects is performed and we use a different sensor for both offline training and online localization phase, we might have an inconsistency between the two data sets. Thus, compensating for hard iron effects is crucial for geomagnetic indoor localization.

Hard iron characteristics can be found by rotating the sensor around its x' , y' , and z' axis. These axes are defined relative to the sensor's reference frame, hence the apostrophe, and

Table I. AVERAGE MAGNETIC FIELD INTENSITY FOR BOTH SENSORS DURING STATIC TEST. VALUES ARE EXPRESSED IN μT .

Intensity	Shimmer	Smartphone
X'	-1.05	0.50
Y'	7.34	19.19
Z'	-57.61	-41.50
F	58.09	42.32

can be found in its documentation. If no hard iron effects are present, rotating a magnetometer 360 degrees and plotting the resulting data as y' axis versus x' axis, will result in a circle centered around the origin. Figures 2 and 3 show the resulting circles of rotating the Shimmer and the smartphone sensor in the $x'y'$ plane, before and after compensating for hard iron effects. Table II shows the compensation values for each axis of both sensors.

After compensating both sensors for these hard iron effects by subtracting the compensation values from the raw data, the first test is repeated. The results are shown in Table III. We can see that both sensors give very similar measurements at the same position.

Often, magnetometers are also calibrated to compensate for the presence of external metal or electronic distortions, called soft iron effects. For this research, this is an undesired calibration as the goal of geomagnetic localization is to measure and map these distortions.

If we do not look at the previous test data, we expect the smartphone to have a higher variance because of its more advanced electronic composition, which might influence the sensitive magnetometer. We note that the shimmer sensor has a slightly larger variance, which is unexpected. Additional tests are conducted with all receivers of the smartphone turned on, in an attempt to maximize the variance. Table IV shows the magnetic field intensity measurements of the smartphone with receivers disabled and enabled. Note that the Bluetooth

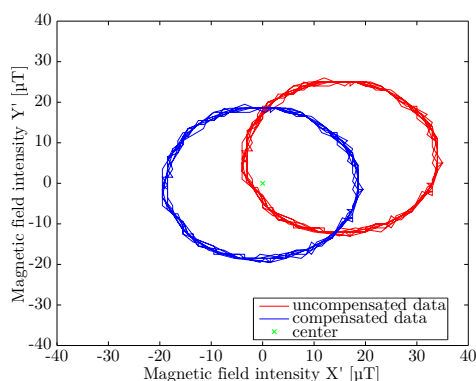


Figure 2. Shimmer hard iron compensation.

Table II. HARD IRON COMPENSATION FOR BOTH SENSORS. VALUES ARE EXPRESSED IN μT .

Correction	Shimmer	Smartphone
X'	15.00	3.67
Y'	7.25	0.16
Z'	-11.25	4.52

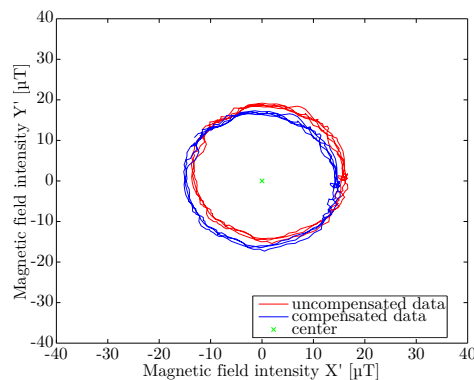


Figure 3. Smartphone hard iron compensation.

Table III. AVERAGE MAGNETIC FIELD INTENSITY AND CORRESPONDING STANDARD DEVIATION FOR BOTH SENSORS DURING STATIC TEST, AFTER HARD IRON COMPENSATION. VALUES ARE EXPRESSED IN μT .

Intensity	Shimmer		Smartphone	
	μ	σ	μ	σ
X'	-0.33	0.56	-0.80	0.48
Y'	17.12	0.52	18.01	0.51
Z'	-45.97	0.57	-44.46	0.51
F	49.06	0.57	47.98	0.52

receiver is enabled in both scenarios as it is used to send back the data to the computer. Although the variance in the data rises slightly when both receivers are activated, it does not significantly affect our measurements.

As the focus of the localization research is handheld smartphones, tests are conducted to see if human hand contact would significantly affect the measurements. During the offline calibration phase measurements can be taken either with or without contact by a human hand. Magnetic field intensity measurement are taken with and without contact by a human hand, without changing the position of the hand. The results of the 200 samples are presented in Table V. The test results show that there was no significant change between both scenarios.

Table IV. AVERAGE MAGNETIC FIELD INTENSITY AND CORRESPONDING STANDARD DEVIATION FOR THE SMARTPHONE MAGNETOMETER, WITH OR WITHOUT ADDITIONAL ELECTRONIC ACTIVITY. VALUES ARE EXPRESSED IN μT .

Intensity	Wi-Fi and GPS disabled		Wi-Fi and GPS enabled	
	μ	σ	μ	σ
X'	15.07	0.47	15.14	0.48
Y'	2.35	0.43	2.43	0.54
Z'	-32.94	0.49	-32.91	0.55
F	36.31	0.50	36.32	0.56

Table V. AVERAGE MAGNETIC FIELD INTENSITY AND CORRESPONDING STANDARD DEVIATION FOR THE SMARTPHONE MAGNETOMETER, WITH OR WITHOUT HUMAN HAND CONTACT. VALUES ARE EXPRESSED IN μT , DIFFERENCES IN %.

Intensity	No hand contact		Hand contact		Difference	
	μ	σ	μ	σ	$\Delta\mu$	$\Delta\sigma$
X'	14.33	0.55	14.48	0.48	98.96	114.58
Y'	1.21	0.50	0.93	0.55	130.11	90.91
Z'	-33.80	0.52	-33.32	0.52	101.44	100.00
F	36.74	0.54	36.35	0.51	101.07	105.88

3) *Indoor magnetic field intensity*: While indoor environments pose good candidates for geomagnetic localization, magnetic field intensity measurements must be stable over long periods of time. [10] conducted experiments where indoor magnetic field intensity was measured in different environments. The results show stable magnetic field intensity measurements over a 24 hour period. The experiments are repeated three months later, and no significant change was detected.

To achieve indoor localization, it is important that magnetic field intensities change considerably from position to position. If the magnetic field intensity measurements do not change considerably, the fingerprint might not contain enough information to overcome the cumulative error of the estimated position and indoor localization cannot be achieved [2].

A dynamic test is performed to see if magnetic field intensity measurements vary over the length of two hallways. The Shimmer sensor is placed on an office chair and is elevated to a height of 1.2 m. This height is similar to a person holding a smartphone. The elevation also made sure there is as little interference as possible from the chair itself.

The chair is moved at a constant velocity of 0.3 cm/s through the hallway. The speed is not always constant as human error is inevitable. The first hallway is expected to have changing measurement values because of the reinforced concrete floor and metal furniture in the rooms next to the hallway. The second hallway is expected to have less varying measurements because of the wooden floor and the absence of metal furniture.

Figures 4 and 5 show the measurements of the X' , Y' , and Z' intensities taken through respectively the first hallway and the second hallway. The test results show changing magnetic field intensity measurements for hallway A. These peaks and drops in magnetic field intensity allow us to identify certain areas inside the hallway and accordingly allow for localization. The measurements of hallway B tell a different story. Since there are no distinct fluctuations to identify certain areas, accurate localization seems improbable.

Additionally, indoor environments are places where objects are often moved or replaced. This will result in changes in the magnetic field intensity maps, decreasing localization

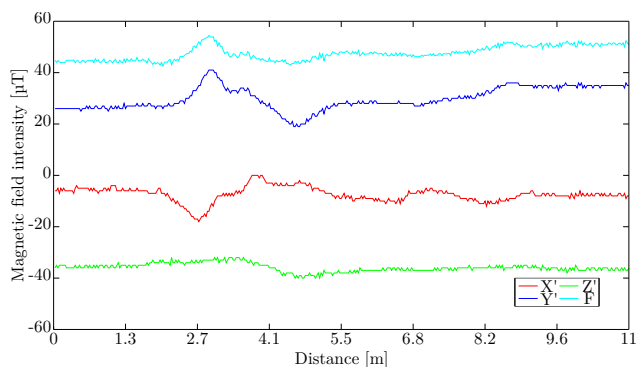


Figure 4. Magnetic field intensity dynamic test of hallway A.

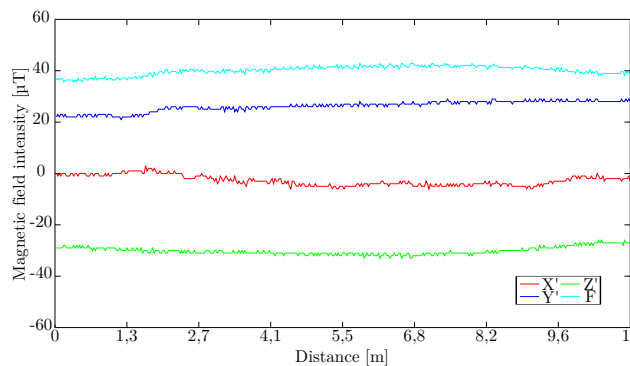


Figure 5. Magnetic field intensity dynamic test of hallway B.

performance, as discussed below.

Tests are conducted to investigate these interferences. Three objects are tested: a perforator, a mobile phone, and a hard drive. These objects are chosen because they can represent normal household objects which are often moved within an indoor environment. These differently sized objects are moved at a constant speed towards a Shimmer sensor to investigate the range and magnitude of the interferences. Figure 6 shows the results of the hard drive test. The hard drive is moved closer to the sensor at a constant speed, reaching the sensor after 50 s. Magnetic field intensity changes drastically as the hard drive moves closer to the sensor. As can be expected the change in magnetic field intensity was less significant for the smaller objects. Table VI shows the interference range of all objects.

Test results show that the size and magnetic composition of the object determines the range and magnitude of the interference. Small sized objects only caused interference starting from a range of about 15 cm, while larger objects

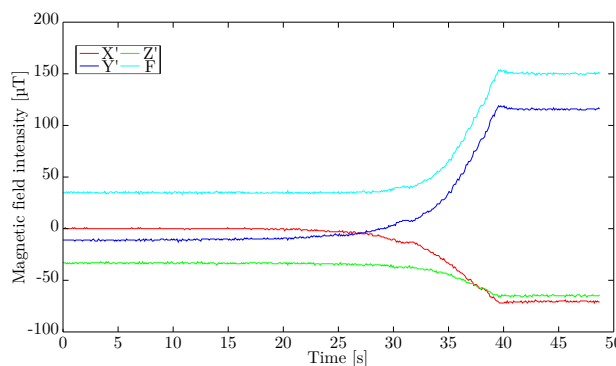


Figure 6. Metal and electronic object interference test of the hard drive.

Table VI. METAL AND ELECTRONIC OBJECT INTERFERENCE TEST RESULTS.

Object	Perforator	Phone	Hard drive
Average velocity [cm/s]	1.48	1.66	1.37
Start of interference [s]	29.00	24.00	23.00
Interference range [cm]	12.00	15.10	23.50

cause interference starting from about 25 cm. Small objects have a negligible influence for a room sized environment, yet the interference of larger objects cannot always be ignored.

B. Fingerprinting

In radio frequency (RF) based localization, fingerprinting is performed by measuring a pattern of RF signals and matching them to a database of such measurements. These measurements are called RF fingerprints, and consist of all pairs of received signal strength (RSS) value and media access control (MAC) address that can be seen at a certain location. This idea was originally published in [26].

Fingerprinting localization has an offline and an online phase. During the offline phase, fingerprints are recorded at reference locations and stored in a database. These fingerprints together form a radio map of the environment, which is used during the online phase. During this online phase, devices that need to be localized measure fingerprints at their location and compare these fingerprints with the radio map in the database. Due to measurement noise and fluctuations in RF signals, these fingerprints are usually not exactly the same as fingerprints in the the database, so a set of measurements is used to estimate a true location. This method is described in more detail in [3].

As shown by [8], this localization technique can be directly applied to magnetic field localization. Instead of RF fingerprints, magnetic field fingerprints are used, by measuring the X , Y , and Z intensities of the geomagnetic field vector B_m , as explained above.

As described in [1], magnetic field intensity maps were created by measuring the magnetic field intensity at predefined locations. The sensor remained still during these measurements.

Three different locations are chosen for experimentation: the ground floor of a suburban house, with an area of 14×16 m; the second floor of a city centered apartment, with an area of 9×12 m; and the second floor lab at the university campus, with an area of 6×19 m. These locations are chosen because they represent distinct environments where indoor localization might be required. It is important that all locations have multiple rooms and are medium to large size, i.e., above 20 m^2 . Figure 7 shows the recorded fingerprints of the suburban house. A slash is drawn through areas where no fingerprint measurement could be obtained because of built in cabinets, wardrobes or other furniture. For simplicity, the color map shows only the magnetic field F intensity measurements taken at one meter spacing. We do not explicitly research the maximum accuracy of geomagnetic localization for this feasibility research.

The fingerprint in Figure 7 shows that the magnetic field intensity characteristics change from position to position. There is a big metal stove located between the dining room and the kitchen. We measured a high magnetic field intensity at that location, which results in a light square. A test is done to determine if these characteristics are unique for an indoor environment. A fingerprint is created in a garden, with an area of 4×6 m, and in a small part of a street, with an area of

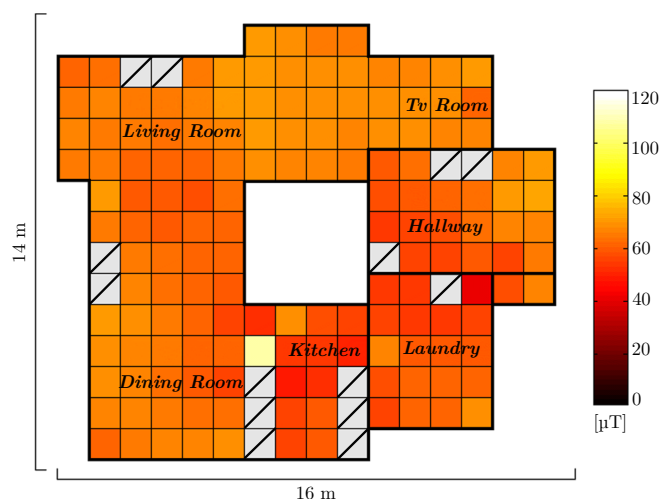


Figure 7. Magnetic field F intensity fingerprint map of the ground floor of the suburban house.

5×15 m. Figure 8 shows the fingerprint obtained at the street. The outdoor results are very different from the indoor results. The magnetic field intensities do not change significantly with position. Tables VII and VIII show the magnetic field intensity standard deviation of the recorded measurements for both the indoor and the outdoor fingerprints. The indoor environments clearly have more varying measurements than the outdoor environments.

Fingerprint maps are also created to confirm the findings on metal and electronic objects' interference mentioned above. A fingerprint is taken from a small bedroom with an area of 3.5×3.5 m. Magnetic field intensity measurements of the X' , Y' , and Z' intensity are taken at 0.5 m spacing. Figure 9 shows the interior setup of the room and the resulting magnetic field intensity fingerprint of the F intensity. As it can be seen from this fingerprint, the two speakers cause a clear magnetic field intensity interference pattern. The size of this distortion

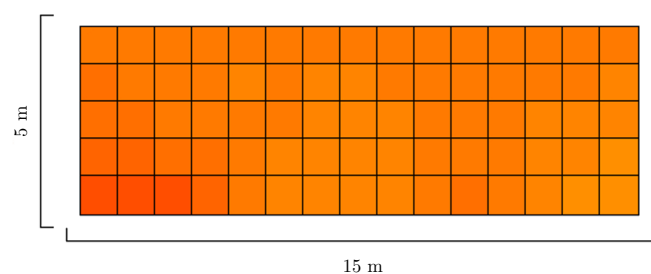


Figure 8. Magnetic field intensity fingerprint map of a part of a street. The intensity color scale is the same as in Figure 7.

Table VII. MAGNETIC FIELD INTENSITY STANDARD DEVIATION VALUES FOR INDOOR LOCATIONS. VALUES ARE EXPRESSED IN μT .

Intensity	House	Apartment	Lab
X'	5.70	5.49	6.99
Y'	4.63	5.52	4.84
Z'	5.11	4.65	8.08

Table VIII. MAGNETIC FIELD INTENSITY STANDARD DEVIATION VALUES FOR OUTDOOR LOCATIONS. VALUES ARE EXPRESSED IN μT .

Intensity	Garden	Street
X'	1.45	3.53
Y'	1.28	3.30
Z'	0.55	2.65

is rather large, as speakers are often constructed with strong magnets inside of them. After creating the first fingerprint map, one of the speakers was moved to a different location within the room. Subsequently, a new fingerprint map was created.

Figure 10 shows the new interior setup and the resulting new fingerprint. The interference pattern of the moved speaker is clearly visible in the new fingerprint. These test results give an example of how the repositioning and removal of objects inside a room can form an obstacle for indoor geomagnetic localization. When the interior setup of a room changes significantly, a new fingerprint should be taken. Of course, a SLAM algorithm could perform continuous mapping of the environment, while simultaneously performing localization.

C. RatSLAM

RatSLAM is a biologically inspired SLAM algorithm, modeled after spatial cognition in rats [27, 28]. It consists of three elements, called the local view network, the pose cell network, and the experience map, as shown in Figure 11. We will give a brief overview of the pose cell network and the experience map, and refer the reader to [28] for additional details. We do present a more in-depth discussion of the local view network as this is the only component that is modified for this research.

1) *Pose cell network*: The pose cell network is a three dimensional continuous attractor network (CAN) [29, 30], representing pose consisting of position in the plane (x, y) and orientation (θ). The activity pattern in this network represents the local pose estimate, or estimates if the pose is ambiguous. It can be visualized as a cube in which activity packets are created, moved around and destroyed. The connectivity pattern between the nodes in a CAN is such that activity packets can be considered as discrete blobs of activity that keep their shape when moved around the network. The activity packets in the pose cell network are moved in accordance with the

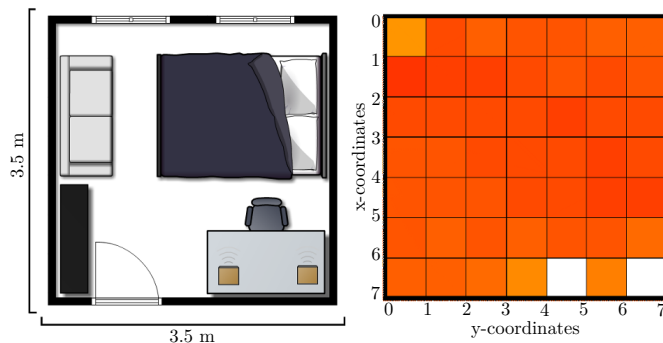


Figure 9. Magnetic field intensity fingerprint of bedroom, with the speaker on its original position. The intensity color scale is the same as in Figure 7.

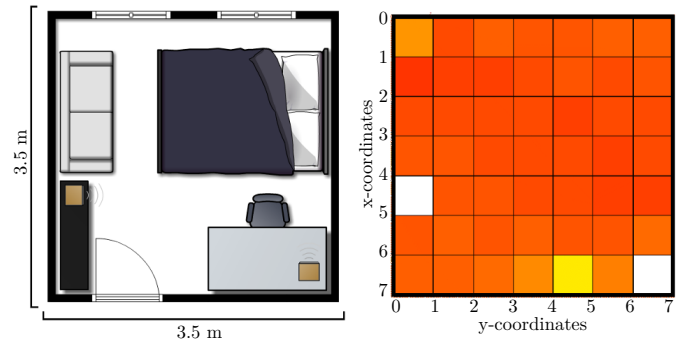


Figure 10. Magnetic field intensity fingerprint of bedroom, with the speaker on its new position. The intensity color scale is the same as in Figure 7.

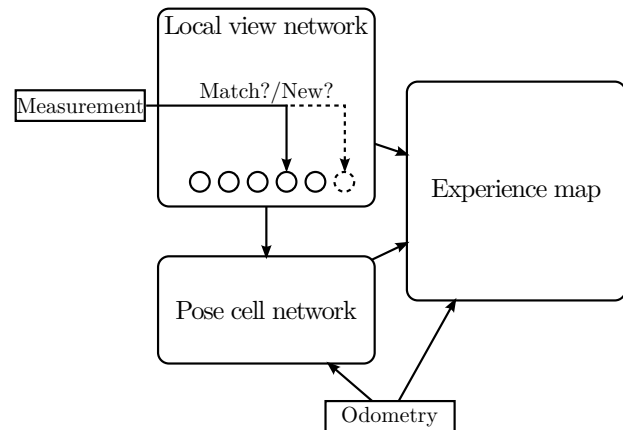


Figure 11. RatSLAM consists of three elements, called the local view network, the pose cell network, and the experience map.

odometry information. The boundaries of the network are wrapped around, so that an activity packet that reaches the end of the network is wrapped back to the start. Hence, multiple positions and orientations in the real world are mapped upon the same nodes in the pose cell network. Extra activity is injected by the local view network, i.e., new activity packets are created when new sensor measurements correspond with memorized sensory signatures, as explained below.

2) *Experience map*: The experience map is a graph that represents a global topological map of the environment, based on information from the local view network, the pose cell network, and the odometry information. It creates new nodes based on the state of the local view network and connects them with new edges to nodes already present in the experience map by using the metric odometry information. This information is continuously updated on the basis of new sensor data, the state of the local view network and activity in the pose cell network. Hence, this topological map acquires semi-metric properties, i.e., progressively more accurate (x, y) coordinates are associated with the nodes that lie on paths that have been repeatedly traveled. A detailed overview of the functioning of the experience map can be found in [31].

3) *Local view network*: The local view network acts as a database of scenes that have been observed during the exploration of the environment. The measurement (see Figure 11) contains the sensor information about the current scene; typically, the measurement is a camera image. When a new measurement is taken, it is compared with previous measurements as stored in the local view templates associated with the local view cells. The activation of each local view cell depends on the quality of this match. If the smallest difference between the measurement and the local view cells is greater than a certain threshold, the measurement is said to correspond with an as yet unobserved scene. In that case, a new local view cell is created and the measurement is copied into the associated local view template. The local view cell is also linked to the position of the activity packet, i.e., the local pose estimate, in the pose cell network that is at that time the dominant packet. Alternatively, if the difference between the measurement and the local view cells is smaller than the threshold, a match is said to be found with the local view cell that had the smallest difference with the measurement. In this case, the local view network will inject activity into the pose cell network at the pose linked previously with this local view cell.

When traveling through previously mapped terrain, a sequence of familiar scenes will be observed by the sensor. However, if the state of the pose cell network differs too much from the true position this will result in the creation of a new activity packet. Indeed, activity being injected in the particular order at the particular places in the pose cell network corresponding with this sequence of familiar scenes will effectively increase the activity in the newly created activity packet. Subsequently, this activity packet will become the strongest and the specific mechanics of the pose cell network will suppress the old activity packet. This mechanism avoids cumulative build-up of odometric errors in the pose estimate when traveling through familiar terrain. Again, more details can be found in the literature [17, 18, 27, 28, 31].

The typical camera image that serves as measurement in the original RatSLAM implementation has been replaced by several other sensor modalities: a biomimetic sonar system modeled after the echolocation abilities of bats [19, 20], the fusion of a laser range finder, a simple sonar array, a depth camera and a normal camera [21]. In this research, we propose to replace the camera images with magnetic field fingerprints as used in the magnetic field localization system.

III. METHOD

In this section, we will discuss the methods used to perform both geomagnetic localization and geomagnetic RatSLAM. Slightly updated, the section on geomagnetic localization is also presented in [1].

A. Geomagnetic localization

The magnetic field intensity results discussed above suggest that magnetic field intensity measurements can be used to

achieve indoor localization. It is important to note, however, that the quality of the localization often depends on the number of measured components that can be used as reference points [2]. Having many values to compare against can obviously increase the chance of identifying the actual position. The number of components that can be recorded by a magnetometer is rather small. Only the X' , Y' , and Z' intensities of the earth's magnetic field, in the reference frame of the magnetometer, can be measured. There are some practical consequences to be considered during the localization and fingerprinting phase when using these three intensities.

As stated before, a magnetometer will measure the magnetic field intensities relative to its own orientation. So, to use the three intensities requires that the orientation of the sensor is exactly the same during the fingerprinting and the localization phase. This is a requirement that cannot be met easily. A user will walk around in different directions and the orientation of the device will follow along with him. The way the user holds the device is also not always the same. Determining the orientation of the device will be key to using all three components. If no information is available about the orientation of the device in none of these two phases, we can only use the F intensity. This would reduce the number of components to be used for localization to only one.

To resolve this issue, a tilt compensated magnetometer can be used. Such a magnetometer uses accelerometers to detect the vertical orientation of the device by measuring the force of the earth's gravity. Using tilt compensation allows us to use two components, the Z intensity and the H' intensity [10]. To use all three components the horizontal orientation of the device needs to be known as well. To determine the horizontal orientation, the magnetometer can be used as a compass. A compass can determine the direction of the magnetic north, and can consequently determine the horizontal orientation of the device. To do this, the user has to manually point the device to a reference point on the map, e.g., geographic north. By defining a reference point the horizontal orientation can be determined.

This research shows, however, that indoor environments can cause interference in the magnetic field intensity measurements. These interferences are called soft-iron effects. Compensation has to be done to remove these interferences to get an accurate heading. It is important to note, that when soft-iron compensation is done, there needs to be a clear distinction between the compensated data and the raw data. Orientation requires soft-iron compensation while localization requires no soft-iron compensation.

All aforementioned information can be combined to define a measurement model for geomagnetic indoor localization. Defining a measurement model can provide a technology interface for sensor fusion systems [3]. Algorithm 1 describes the measurement model. The measurement model is used to find the probability of a position $\mathbf{x}_t = \{x_t, y_t\}$, where x and y are spatial coordinates, given a measurement \mathbf{z}_t , which can be any of:

$$\mathbf{z}_t = \{z_t^X, z_t^Y, z_t^Z\} \quad (3)$$

$$\mathbf{z}_t = \{z_t^{H'}, z_t^Z\} \quad (4)$$

$$\mathbf{z}_t = \{z_t^F\} \quad (5)$$

where X , Y , and Z indicate intensities of the magnetic B field. Equation (3) can be used when both tilt compensation and heading compensation are performed. Equation (4) can be used when only tilt compensation is performed. Equation (5) can be used when no compensation is performed. The algorithm uses a Gaussian kernel distribution $p(z_t^k | \mathbf{x}_t)$:

$$p(z_t^k | \mathbf{x}_t) = \exp\left(\frac{z_t^k - z_{dB}^k}{2 * \sigma^2}\right) \quad (6)$$

where z_{dB} is the fingerprint in the database corresponding with \mathbf{x}_t and k is any of X , Y , Z , H' , or F .

Algorithm 1 Geomagnetic measurement model ($\mathbf{x}_t, \mathbf{z}_t$).

```

1: function CALCULATEWEIGHT( $\mathbf{x}_t, \mathbf{z}_t$ )
2:   if  $\mathbf{z}_t == \{z_t^X, z_t^Y, z_t^Z\}$  then
3:      $w_X = p(z_t^X | \mathbf{x}_t)$ 
4:      $w_Y = p(z_t^Y | \mathbf{x}_t)$ 
5:      $w_Z = p(z_t^Z | \mathbf{x}_t)$ 
6:     return  $w_X \cdot w_Y \cdot w_Z$ 
7:   else if  $\mathbf{z}_t == \{z_t^{H'}, z_t^Z\}$  then
8:      $w_{H'} = p(z_t^{H'} | \mathbf{x}_t)$ 
9:      $w_Z = p(z_t^Z | \mathbf{x}_t)$ 
10:    return  $w_{H'} \cdot w_Z$ 
11:  else if  $\mathbf{z}_t == \{z_t^F\}$  then
12:     $w_F = p(z_t^F | \mathbf{x}_t)$ 
13:    return  $w_F$ 
14:  end if
15: end function

```

Although magnetic field intensity measurements remain stable over long periods of time, big, moving metal objects like an elevator cause variations in these measurements. These sources of errors can cause a mismatch in the magnetic field intensity measured at the same position. The accumulated error can be modeled as a Gaussian kernel distribution. The standard deviation of this distribution has to represent the maximum variation that can be expected. The standard deviation σ was set to $2 \mu\text{T}$ as this was the maximum standard deviation reported at 2 m from an elevator by [10].

B. Geomagnetic RatSLAM

We use our Pioneer 3DX mobile robot to collect measurements and to provide a reliable odometry source for our geomagnetic RatSLAM implementation. The Pioneer 3DX serves as robot platform, with a consumer grade laptop mounted on top to save the measurements. Elevated by a cardboard box, we place our sensor at a safe distance to avoid soft iron interference in the magnetic field caused by the metal parts of the robot. The setup is shown in Figure 12. The robot is also equipped with a laser range finder to serve as a

comparison tool using an established laser range finder based SLAM method.

The local view network of the original RatSLAM algorithm uses camera images to recognize scenes. This functionality has to be replaced with an algorithm capable of recognizing magnetic field intensity measurements. Assuming that our magnetometer will always be in the same position relative to the robot, we can simplify the measurement model. Similar to how a 60° angle of view camera can only observe one direction at a time, we choose to match only to magnetic field intensity measurements that are oriented in the same way during initial measurement and during subsequent comparison. In other words, our algorithm will not attribute a high match quality to the measurements from one location when it is being traversed in a different orientation. This results in \mathbf{z}_t to have only one option:

$$\mathbf{z}_t = \{z_t^{X'}, z_t^{Y'}, z_t^{Z'}\} \quad (7)$$

which is different from Equations (3), (4), and (5) by always using the magnetometer reference frame defined by X' , Y' , and Z' , which is allowed since we only want matches when the magnetometer has the same orientation for the measurements being compared. In fact, we can assume $Z' = Z$, since Z' is always oriented to nadir. We do not explicitly model it that way, however, so that our approach is more general even for differently oriented magnetometers. The same Gaussian kernel distribution $p(z_t^k | \mathbf{x}_t)$ as in Equation (6) is used, with $\sigma = 0.67 \mu\text{T}$. This difference in standard deviation is created to be more selective in matching local view cells.

We use the Robot Operating System (ROS, [32]) as a framework to read magnetometer messages from the smartphone and to operate the robot. The freely available OpenRatSLAM source code [31] is modified to create RatSLAM results.

IV. RESULT

Here, we will present the results we have obtained for both geomagnetic localization and geomagnetic RatSLAM. Firstly, the geomagnetic localization results are shown, originating with slight modification from the original paper [1]. Next, we present the new geomagnetic RatSLAM results.



Figure 12. The Pioneer 3DX mobile robot platform.

A. Geomagnetic localization

The measurement model in Algorithm 1 is used to investigate the feasibility of geomagnetic indoor localization. To test the feasibility we use the suburban house, the apartment, and the university lab as experimental environments. Each individual fingerprint position and its accompanying magnetic field intensity measurement is used as a test position. Each test position is compared to all measurement positions in the fingerprint using the measurement model described in Algorithm 1. The measurement model will give a high weight to fingerprint positions that had magnetic field intensity measurements similar to the test position. The weight represents the likelihood of the sensor reading z_t given the position x_t . The final estimated position x_t is calculated as the weighted average of all fingerprint positions, using Equation (8). Positions with a high probability will contribute more to the final estimated position [3].

$$x_t = \frac{\sum_{i=1}^N w_t^{[i]} \cdot x_t^{[i]}}{\sum_{i=1}^N w_t^{[i]}} \quad (8)$$

where N is the number of positions.

The coordinates of the final estimated position are compared to the real coordinates of the test position and the error is stored. The process will be repeated for all measurement positions within the fingerprint. The maximum, minimum and average errors for every location are determined. The amount of estimated positions that are within 1 m and the amount of estimated positions that are in the same room is also determined. Table IX shows the results that are obtained from the three fingerprints that are recorded.

It is clear from the results that using three components gives the best localization results and results deteriorate when fewer components are used. The maximum and minimum errors stay relatively the same for all amounts of components. All localization results are combined to form a cumulative density function in Figure 13.

This test is repeated, with this difference that the room of each test position is known. Table X shows the results of this test. Only measurement positions in the same room as the test positions are compared to the test position. Test results improve significantly, so that even using only one component, localization close to 1 m can be achieved. These results indicate that geomagnetic localization might be more suited for localization within a room. Figure 14 show the cumulative density function when the room is known.

Table IX. GEOMAGNETIC LOCALIZATION FEASIBILITY RESULTS FOR DIFFERENT ENVIRONMENTS, USING ONE, TWO, OR THREE COMPONENTS IN THE MEASUREMENTS MODEL.

Properties	Suburban house			Apartment			Lab		
	1	2	3	1	2	3	1	2	3
mean [m]	4.8	4.3	3.1	3.7	3.3	2.5	4.5	3.4	2.5
min [m]	0.1	0.0	0.0	0.1	0.1	0.0	0.2	0.0	0.0
max [m]	9.3	9.4	8.8	7.2	7.4	7.0	10.5	11.3	11.8
< 1 m [%]	4.0	9.0	17.0	7.0	13.0	23.0	9.0	20.0	32.0
room [%]	10.0	18.0	44.0	21.0	31.0	49.0	73.0	74.0	82.0

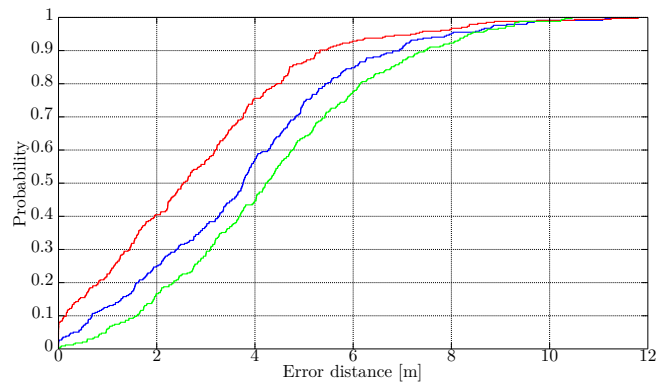


Figure 13. Cumulative density function of the error of localization. The green line is using one component; the blue line is using two components; the red line is using three components.

Table X. GEOMAGNETIC LOCALIZATION FEASIBILITY RESULTS WHEN THE ROOM IS KNOWN FOR DIFFERENT ENVIRONMENTS, USING ONE, TWO, OR THREE COMPONENTS IN THE MEASUREMENTS MODEL.

Properties	Suburban house			Apartment			Lab		
	1	2	3	1	2	3	1	2	3
mean [m]	1.4	1.0	0.8	1.4	1.0	0.6	2.2	1.4	0.9
min [m]	0.1	0.0	0.0	0.0	0.0	0.0	0.1	0.0	0.0
max [m]	3.2	2.8	2.3	5.2	3.9	2.1	5.4	5.2	3.7
< 1 m [%]	30.0	47.0	67.0	35.0	50.0	74.0	21.0	42.0	61.0

Although previous results give a good indication of how feasible geomagnetic indoor localization can be, they are largely theoretical. To verify these findings, a more practical test is performed. A route is recorded through the suburban house. On this route, magnetic field intensity measurements are taken at roughly the same positions as where fingerprint measurements are taken. The position can not be exactly the same as human error is inevitable. Figure 15 shows the recorded magnetic field intensity for the route and the fingerprint.

The results show that the recorded measurements are not exactly the same, however, the average correlation coefficient between the route and the fingerprint X , Y , and Z

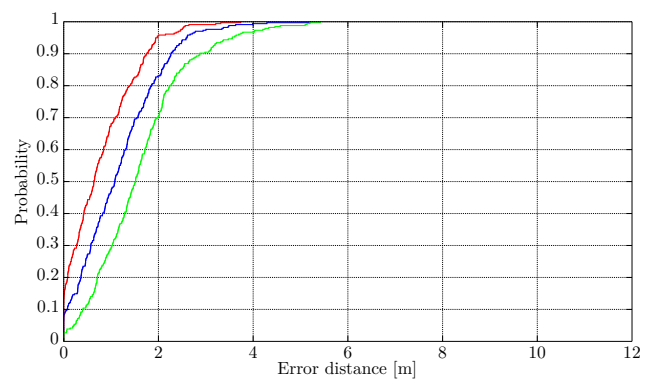


Figure 14. Cumulative density function of the error of localization when the room is known. The green line is using one component; the blue line is using two components; the red line is using three components.

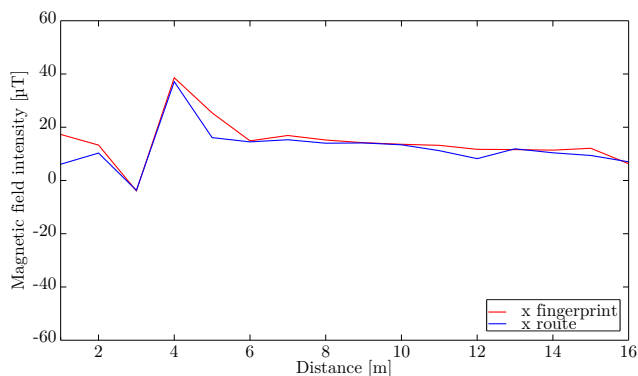


Figure 15. Magnetic field intensity X measurements from fingerprint map and during route.

measurements is 0.93, which means that both recordings are very similar. The recorded route is estimated within the environment using Algorithm 1. Figure 16 shows the original route in blue, and the estimated route in green. First the route is estimated when nothing about the room is known, later the route is estimated when the room of the measurement is known. Table XI shows the localization results of both scenarios.

This practical test confirms the original findings. Localization is very dependent on the amount of components that can be used, and results are superior when only room sized localization is required.

B. Geomagnetic RatSLAM

Our geomagnetic RatSLAM results are collected in the same university lab as the geomagnetic localization results. We do not provide the algorithm with any information about the

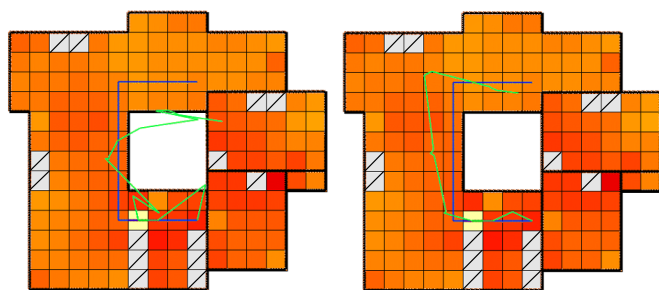


Figure 16. Suburban house route results for three components. Left hand side, when the room was not known. Right hand side, when the room was known. The blue line is the recorded route and the green line is the estimated route. The intensity color scale is the same as in Figure 7.

Table XI. ROUTE ESTIMATION RESULTS.

Properties	Global			Room known		
	1	2	3	1	2	3
mean [m]	2.1	2.1	1.4	1.3	1.1	0.9
min [m]	0.2	0.1	0.0	0.0	0.0	0.0
max [m]	4.22	4.2	4.5	3.1	2.6	2.0
< 1 m [%]	13.0	13.0	38.0	43.0	43.0	62.0
room [%]	25.0	31.0	56.0	N/A	N/A	N/A

specific room in which measurements are taken. A point to point quantitative ground truth is not available for the results, but we show the path produced with only odometry and the path produced by Grid Mapping as qualitative comparisons. The odometry only path is expected to perform much worse, as it has no sensor information to recognize familiar scenes. The Grid Mapping algorithm is freely available in the ROS framework and described in [33]. This path is expected to perform better than our own estimation, since it utilizes the laser range scanner high precision data.

Four separate datasets are constructed. Three of them are simple runs up and down the lab, starting and ending in different rooms, lasting about 15 min each. A fourth dataset drives up and down to different rooms in different order, lasting about 30 min. The first three are used to find the correct RatSLAM parameters, by training on two of them and checking on the third, switching datasets for every parameter setup. This approach does not guarantee that optimal parameters are found, but decreases the chance of overfitting the parameters. To additionally prevent overfitting, the fourth dataset is used as final check. Figure 17 shows a schematic overview of these runs, drawn against the output of the Grid Mapping algorithm applied to the fourth dataset.

The traveled path is the general output of the RatSLAM algorithm. This will be discussed further on for the fourth, challenging dataset, however, our focus was on the local view network. These results are generally discussed using local view cell matching diagrams, which are diagrams on which the local view cell identification number, or template ID, is drawn as a function of time. Horizontally, the first time a template ID is encountered is when the local view cell is created. Subsequent occurrences of the same template ID indicate when the local

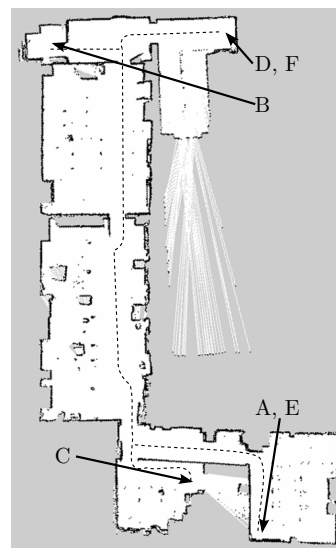


Figure 17. The second floor university lab laser map. The first three datasets consist of three runs going up and down the lab. The first dataset went from A to B and back; the second dataset went from C to D and back; and the third dataset went from E to F and back. The fourth dataset went to all rooms in different order. The general trajectory is shown as a dashed line.

view network decided a measurement to originate from a location encountered before. Similarly, the experience node identification number, or experience ID, is drawn, to indicate when exactly the experience map was informed to create a new location or to link to an existing location.

Figure 18 shows such matching diagrams for the first dataset, using a camera the first time and using magnetometer the second time as input. We observe a similar response in both sensors, where locations encountered while going up the run are found to be different from locations encountered while going down the run. As explained before, this is expected behavior. Three parallel, diagonal lines can be seen in the figure, once for view template matches and once for experience node matches. The first, left hand side of these lines indicates new local view cells or experience nodes being created. The second and third of these lines start when the robot reaches location A again, as indicated in Figure 17, on the 300th and 600th second mark. These lines indicate matches to the originally created view templates or experience nodes. False positive matches are labeled FP on the figure. They can be found between the lines created by correct matches to the originally created view templates.

We also note many more false positive local view cell matches when using the magnetometer. This is explained by the RatSLAM parameters, where we have chosen a local view cell matching threshold for the magnetometer that favors matches, including some false positive matches, above one that finds few matches but avoids finding false positive matches. This parameter setting improves experience node matching, facilitating effective loop closure. A camera does not need this coarse matching threshold, because it has a sample rate six times higher than our magnetometer. Matches will be reported many times more often than with the magnetometer.

The other two initial datasets showed similar results, so we can test the obtained parameters on our more challenging fourth dataset. An overview of our parameters can be found in Table XII. A new local view cell will be created when the weight calculated by our measurement model is lower than the match threshold. The recency threshold prevents the local view network from matching new measurements with recently created local view cells. In other words, with a magnetometer frequency of about 5 Hz, the last eight seconds of measurements are ignored when creating a match. The dimension of the pose cell network is increased to further cope with the false positive local view cell matches. The pose cell injection energy is how much energy is injected into the pose cell network on each local view match. Other parameters are left on their default values. A detailed discussion of these parameters when using the OpenRatSLAM system can be found in [31].

Figure 19 shows the map created using only odometry, using our geomagnetic RatSLAM, and using Grid Mapping. The raw integrated odometry in Figure 19a shows some structure of the environment when observed carefully, however, it can in no way be used for either localization or navigation. The trajectory created using Grid Mapping in Figure 19c shows

Table XII. PARAMETERS USED FOR THE GEOMAGNETIC RATSLAM.

Parameter	Value
Match threshold	0.5
Recency threshold	40
Pose cell xy dimension	37
Pose cell injection energy	0.03

clearly what path has actually been followed by our robot. Do note that this trajectory was created using a high precision laser range finder, in contrast to our simple smartphone magnetometer. The trajectory created using the magnetometer is shown in Figure 19b. It can be divided into two parts, the coarse lower part and the precise upper part. The lower part of the run has fewer experience node matches, i.e., loop closure, so that different traversals of the same location are not matched to each other. The upper part of the run has many more experience node matches, so that different traversals of the same location are matched to each other.

This difference is supported by the template match diagram in Figure 18, where less experience node matches are seen in the region when the robot is near location A (as indicated on Figure 17), which is the 0th, 300th, 600th, and 900th second region. The regions in Figure 17 indicated by A, C, and E are located in a much older section of the building, with wooden floors and thin walls, without any offices. This causes the magnetic field intensity to be only slightly distorted in these regions. Consequently, geomagnetic localization in these regions is difficult.

The upper part of Figure 19b indicates a very precise operation of geomagnetic RatSLAM. This is a more modern region of the building, indicating that geomagnetic RatSLAM is feasible to use as SLAM mechanism in average indoor environments. The created experience map can subsequently be used for both localization and navigation tasks.

V. CONCLUSION AND FUTURE WORK

In this research, we show that the geomagnetic B field is feasible to use in both localization and SLAM applications. We first show an extensive review of platform and sensor independence when measuring the magnetic field intensity. Subsequently, we show localization feasibility with tests in various environments. Lastly, we demonstrate our newly developed geomagnetic input for the local view network of the RatSLAM system.

Our results indicate that geomagnetic localization and geomagnetic RatSLAM is strongly dependent on the environment. Environments with much magnetic field intensity distortion will allow more accurate localization and SLAM. Such environments are rather commonplace for indoor applications: most modern domestic or professional environments hold enough metal and electric devices to distort the geomagnetic field. Environments with little magnetic field intensity distortion will not provide enough information for accurate localization and SLAM.

We also note that geomagnetic localization performs better when used for localization within limited areas, such as rooms.

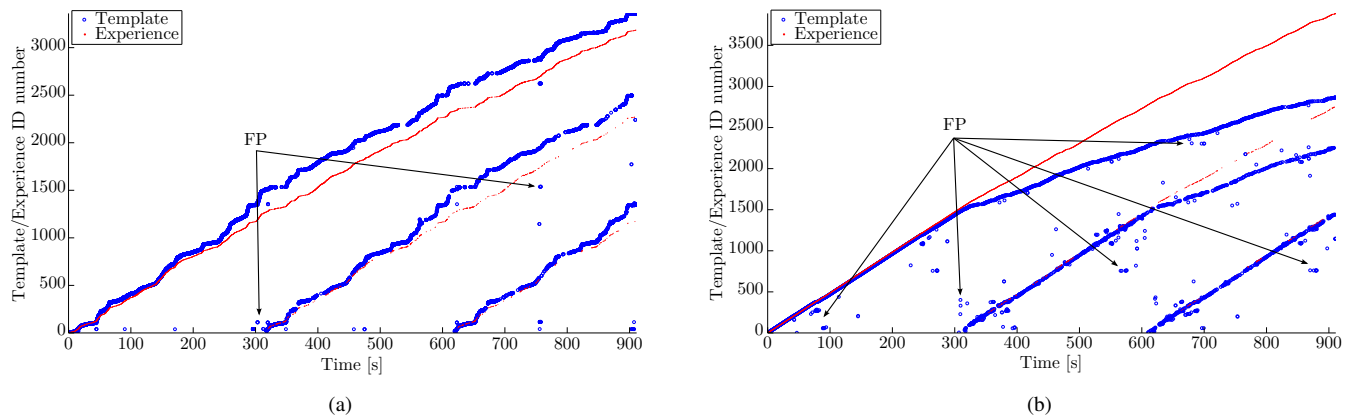


Figure 18. View template and experience matches for the first dataset: (a) shows the view template matches and experience node matches created using camera; and (b) shows the view template matches and experience node matches created using magnetometer.

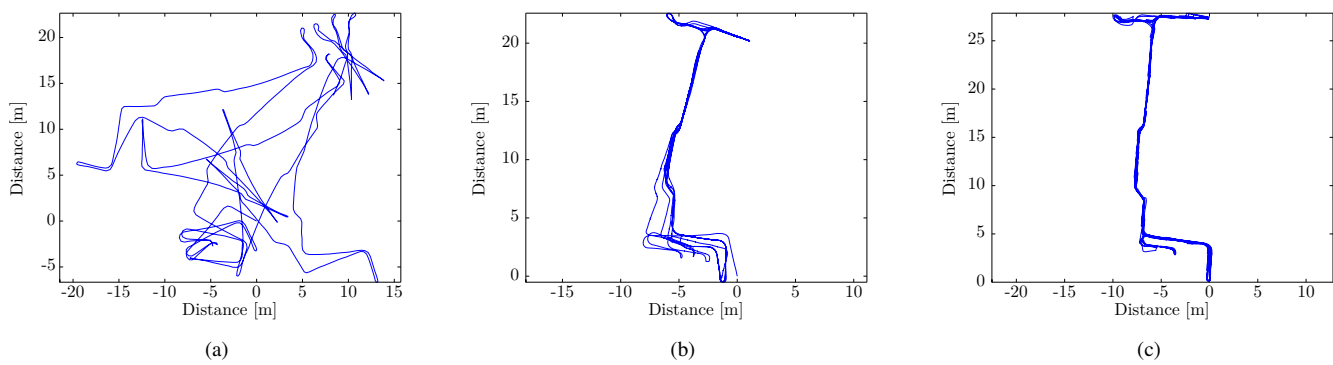


Figure 19. Traveled path for the fourth dataset: (a) shows the raw integrated odometry; (b) shows the experience map created by geomagnetic RatSLAM; and (c) shows the traveled path obtained from using the laser range finder based Grid Mapping algorithm available in ROS.

This suggests a complementarity with Wi-Fi as a localization system, which provides a rather coarse spatial localization and is used usually to locate up to room level [3]. In further research we will focus on fusing the virtues of these systems into the RatSLAM local view network. We will also look into fusing other electromagnetic sensors in the same system.

REFERENCES

- [1] D. Vandermeulen, C. Vercauteren, and M. Weyn, "Indoor localization using a magnetic flux density map of a building," in *The Third International Conference on Ambient Computing, Applications, Services and Technologies*. Porto: IARIA, 2013, pp. 42–49.
- [2] R. Mautz, "Indoor Positioning Technologies," Ph.D. dissertation, Institute of Geodesy and Photogrammetry, 2012.
- [3] M. Weyn, "Opportunistic Seamless Localization," Ph.D. dissertation, University of Antwerp, 2011.
- [4] L. C. Boles and K. J. Lohmann, "True navigation and magnetic maps in spiny lobsters," *Nature*, vol. 421, no. 6918, pp. 60–3, Jan. 2003.
- [5] H. Mouritsen, G. Feenders, M. Liedvogel, and W. Kropp, "Migratory birds use head scans to detect the direction of the earth's magnetic field," *Current biology*, vol. 14, no. 21, pp. 1946–9, Nov. 2004.
- [6] S. Suksakulchai, S. Thongchai, D. Wilkes, and K. Kawamura, "Mobile robot localization using an electronic compass for corridor environment," in *SMC 2000 Conference Proceedings. 2000 IEEE International Conference on Systems, Man and Cybernetics. 'Cybernetics Evolving to Systems, Humans, Organizations, and their Complex Interactions' (Cat. No.00CH37166)*, vol. 5. Nashville, TN, USA: IEEE, 2000, pp. 3354–3359.
- [7] J. Haverinen and A. Kemppainen, "Global indoor self-localization based on the ambient magnetic field," *Robotics and Autonomous Systems*, vol. 57, no. 10, pp. 1028–1035, Oct. 2009.
- [8] W. F. Storms, "Magnetic field aided indoor navigation," DTIC Document, Tech. Rep., 2009.
- [9] J. Chung, M. Donahoe, C. Schmandt, I.-J. Kim, P. Razavai, and M. Wiseman, "Indoor location sensing using geo-magnetism," in *Proceedings of the 9th international conference on Mobile systems, applications, and services - MobiSys '11*. New York, New York, USA: ACM Press, 2011, p. 141.
- [10] B. Li, T. Gallagher, A. G. Dempster, and C. Rizos, "How feasible is the use of magnetic field alone for indoor positioning?" in *Indoor Positioning and Indoor Navigation (IPIN), 2012 International Conference on*. Sydney, Australia: IEEE, Nov. 2012, pp. 1–9.
- [11] M. Frassl, M. Angermann, M. Lichtenstern, P. Robertson, B. J. Julian, and M. Doniec, "Magnetic maps of indoor environments for precise localization of legged and non-legged locomotion," in *Intelligent Robots and Systems (IROS), 2013 IEEE/RSJ International Conference on*. IEEE, Nov. 2013, pp. 913–920.
- [12] H. Durrant-Whyte and T. Bailey, "Simultaneous localization and mapping: part I," *IEEE Robotics & Automation Magazine*, vol. 13, no. 2, pp. 99–110, Jun. 2006.
- [13] T. Bailey and H. Durrant-Whyte, "Simultaneous localization and mapping (SLAM): part II," *IEEE Robotics & Automation Magazine*, vol. 13, no. 3, pp. 108–117, Sep. 2006.
- [14] R. Madhavan and H. F. Durrant-Whyte, "Natural landmark-based autonomous vehicle navigation," *Robotics and Autonomous Systems*, vol. 46, no. 2, pp. 79–95, 2004.
- [15] M. Eich, R. Hartanto, S. Kasperski, S. Natarajan, and J. Wollenberg, "Towards Coordinated Multirobot Missions for Lunar Sample Collection

- in an Unknown Environment,” *Journal of Field Robotics*, vol. 31, no. 1, pp. 35–74, Jan. 2014.
- [16] M. Montemerlo and S. Thrun, *FastSLAM: A scalable method for the simultaneous localization and mapping problem in robotics*, B. Siciliano, O. Khatib, and F. Groen, Eds. Springer Berlin Heidelberg New York, 2007, vol. 27.
- [17] M. Milford and G. Wyeth, “Persistent navigation and mapping using a biologically inspired SLAM system,” *The International Journal of Robotics Research*, vol. 29, no. 9, pp. 1131–1153, 2010.
- [18] —, “Mapping a Suburb With a Single Camera Using a Biologically Inspired SLAM System,” *IEEE Transactions on Robotics*, vol. 24, no. 5, pp. 1038–1053, Oct. 2008.
- [19] J. Steckel, D. Vanderelst, and H. Peremans, “BatSLAM: combining biomimetic sonar with a hippocampal model,” in *Proceedings of the Robotica Conference*, Guimaraes, Portugal, 2012, pp. 81–86.
- [20] J. Steckel and H. Peremans, “BatSLAM: Simultaneous localization and mapping using biomimetic sonar,” *PLoS ONE*, vol. 8, no. 1, p. e54076, Jan. 2013.
- [21] M. Milford and A. Jacobson, “Brain-inspired Sensor Fusion for Navigating Robots,” in *Robotics and Automation (ICRA), 2013 IEEE International Conference on*. Karlsruhe, Germany: IEEE, 2013, pp. 2891–2898.
- [22] I. Vallivaara, J. Haverinen, A. Kemppainen, and J. Roning, “Simultaneous localization and mapping using ambient magnetic field,” in *Multisensor Fusion and Integration for Intelligent Syst. (MFI), 2010 IEEE Conf. on*. IEEE, Sep. 2010, pp. 14–19.
- [23] M. Angermann and P. Robertson, “FootSLAM: Pedestrian Simultaneous Localization and Mapping Without Exteroceptive Sensors—Hitchhiking on Human Perception and Cognition,” *Proceedings of the IEEE*, vol. 100, no. Special Centennial Issue, pp. 1840–1848, May 2012.
- [24] P. Robertson, M. Frassl, M. Angermann, M. Doniec, B. J. Julian, M. G. Puyol, M. Khider, M. Lichtenstern, and L. Bruno, “Simultaneous Localization and Mapping for Pedestrians using Distortions of the Local Magnetic Field Intensity in Large Indoor Environments,” in *Indoor Positioning and Indoor Navigation (IPIN), 2013 International Conference on*. Montbéliard-Belfort, France: IEEE, 2013, p. 10.
- [25] S. Maus, S. Macmillan, S. McLean, B. Hamilton, M. Nair, A. Thomson, and C. Rollins, “The US/UK world magnetic model for 2010–2015,” British Geological Survey, Edinburgh, UK, Tech. Rep., 2010.
- [26] P. Bahl and V. N. Padmanabhan, “RADAR: an in-building RF-based user location and tracking system,” in *INFOCOM 2000. Nineteenth Annual Joint Conference of the IEEE Computer and Communications Societies. Proceedings. IEEE.*, vol. 2. Tel Aviv, Israel: IEEE, 2000, pp. 775–784 vol.2.
- [27] M. Milford, *Robot navigation from nature: Simultaneous localisation, mapping, and path planning based on hippocampal models*, B. Siciliano, O. Khatib, and F. Groen, Eds. Springer, 2008, vol. 41.
- [28] G. Wyeth and M. Milford, “Spatial cognition for robots,” *IEEE Robotics and Automation Magazine*, vol. 16, no. 3, pp. 24–32, Sep. 2009.
- [29] S. M. Stringer, T. P. Trappenberg, E. T. Rolls, and I. E. T. de Araujo, “Self-organizing continuous attractor networks and path integration: one-dimensional models of head direction cells,” *Network: Computation in Neural Syst.*, vol. 13, no. 2, pp. 217–42, May 2002.
- [30] S. M. Stringer, E. T. Rolls, T. P. Trappenberg, and I. E. T. de Araujo, “Self-organizing continuous attractor networks and path integration: two-dimensional models of place cells,” *Network: Computation in Neural Syst.*, vol. 13, no. 4, pp. 429–46, Nov. 2002.
- [31] D. Ball, S. Heath, J. Wiles, G. Wyeth, P. Corke, and M. Milford, “Open-RatSLAM: an open source brain-based SLAM system,” *Autonomous Robots*, pp. 1–28, Feb. 2013.
- [32] M. Quigley, K. Conley, B. Gerkey, T. Foote, J. Leibs, R. Wheeler, and A. Ng, “ROS: an open-source Robot Operating System,” in *ICRA workshop on open source software*, vol. 3, no. 3.2, 2009.
- [33] G. Grisetti, C. Stachniss, and W. Burgard, “Improved Techniques for Grid Mapping With Rao-Blackwellized Particle Filters,” *IEEE Transactions on Robotics*, vol. 23, no. 1, pp. 34–46, Feb. 2007.